Methods xxx (xxxx) xxx–xxx

Contents lists available at ScienceDirect

Methods

journal homepage: www.elsevier.com/locate/ymeth

Nanoscale exploration of the extracellular space in the live brain by combining single carbon nanotube tracking and super-resolution imaging analysis

Chiara Paviolo[a,b,1], Federico N. Soria[c,d,1], Joana S. Ferreira[e,f,1], Antony Lee[a,b], Laurent Groc[e,f], Erwan Bezard[c,d], Laurent Cognet[a,b,*]

[a] Université de Bordeaux, Laboratoire Photonique Numérique et Nanosciences, UMR 5298, 33400 Talence, France
[b] Institut d'Optique & CNRS, LP2N UMR 5298, 33400 Talence, France
[c] Université de Bordeaux, Institut des Maladies Neurodégénératives, UMR 5293, 33076 Bordeaux, France
[d] CNRS, IMN UMR 5293, 33076 Bordeaux, France
[e] Université de Bordeaux, Interdisciplinary Institute for Neurosciences, UMR 5297, 33076 Bordeaux, France
[f] CNRS, IINS UMR 5297, 33076 Bordeaux, France

ARTICLE INFO

Keywords:
Single-walled carbon nanotubes
Near-infrared microscopy
Organotypic brain slices
Acute brain slices
Live imaging
Local diffusivity
Single molecule detection

ABSTRACT

The brain extracellular space (ECS) is a system of narrow compartments whose intricate nanometric structure has remained elusive until very recently. Understanding such a complex organisation represents a technological challenge that requires a technique able to resolve these nanoscopic spaces and simultaneously characterize their rheological properties. We recently used single-walled carbon nanotubes (SWCNTs) as near-infrared fluorescent probes to map with nanoscale precision the local organization and rheology of the ECS. Here we expand our method by tracking single nanotubes through super-resolution imaging in rat organotypic hippocampal slices and acute brain slices from adult mice, pioneering the exploration of the adult brain ECS at the nanoscale. We found a highly heterogeneous ECS, where local rheological properties can change drastically within few nanometres. Our results suggest differences in local ECS diffusion environments in organotypic slices when compared to adult mouse slices. Data obtained from super-resolved maps of the SWCNT trajectories indicate that ECS widths may vary between brain tissue models, with a looser, less crowded nano-environment in organotypic cultured slices.

1. Introduction

The extracellular space (ECS) is a system of interconnected compartments limited by cellular membranes containing the interstitial fluid, a local version of the cerebrospinal fluid consisting of water, solutes and the extracellular matrix (ECM). The ECS constitutes 20% of the total brain volume [1,2] and its role in brain physiology is well established as a dynamic pool and diffusive medium for ions, neurotransmitters and other signalling molecules [3,4]. Despite the relevance of this often neglected part of the brain, its dynamics and structural organisation at nanoscale temporal and spatial resolution still represent a knowledge frontier in brain research [5]. This is in striking contrast with the outstanding achievements probing the intracellular [6] and membrane compartments [7] brought by the recent developments in the super-resolution microscopy field.

Our lack of information about the ECS topology is mostly due to insufficient appropriate tools to explore it. With a width in the nanometre range and lack of defined molecular entities to label it, the ECS has remained a dark area in neuroscience for many years. Until very recently, most topological data from the ECS had been obtained by electron microscopy (EM), a technique that gives information on the local topology at the sub-micron resolution. However, fixation and dehydration methods for EM tend to shrink the ECS and underestimate its size. The use of sucrose [8] or sodium cacodylate [9] in the fixative solution, or recently more elegant cryofixation techniques [2,10] have attempted to solve this problem, successfully preserving the ECS ultrastructure. Nevertheless, the fixation requirements impede EM techniques to analyse the dynamics of the ECS and its interplay with physiological processes in real time. This is where light microscopy, live imaging and biophysics come into play, which together with super-

* Corresponding author at: Université de Bordeaux, Laboratoire Photonique Numérique et Nanosciences, UMR 5298, 33400 Talence, France.
E-mail address: laurent.cognet@u-bordeaux.fr (L. Cognet).
[1] These authors contributed equally.

https://doi.org/10.1016/j.ymeth.2019.03.005
Received 2 January 2019; Received in revised form 4 March 2019; Accepted 7 March 2019

resolution methods have started to unveil the fine complex organisation of the ECS in live brain tissue.

Understanding local diffusion in the brain is as important as knowing its nanoscale topology. Brain signalling through ions, neurotransmitters, and large molecules such as neuropeptides or cytokines, depends on the local diffusive properties of the ECS [1,11]. The spatiotemporal profile of molecular mobility in relation to the nanoscopic dimensions of the ECS is poorly understood, and we still do not grasp completely how local diffusion is regulated in the brain ECS. To tackle this question, several efforts have emerged in the neuroscience and biophysics community. Nicholson *et al.* used an integrative optical imaging approach to measure the effective diffusion coefficients of dextran molecules in the ECS of rat cortical slices, hence estimating the values of ECS tortuosity [12]. Moreover, several studies combining real-time iontophoresis and modelling revealed and interpreted ECS volume fraction and tortuosity in both awake and anesthetised animals [5].

In a recent paper, we described for the first time the local nanoscale organisation and diffusion environment of the brain ECS in rat pups, by single-molecule tracking of carbon nanotubes in *ex vivo* acute brain slices [13]. Single-walled carbon nanotubes (SWCNTs) are near-infrared luminescent probes suitable for biological imaging, displaying exceptional brightness and photostability in water [14,15]. Due to their large aspect ratio (more than 100 nm of length versus 1 nm in diameter), SWCNTs are able to disseminate over long distances in crowded environments by reptation for micrometer-long nanotubes diffusing in sub-micrometer size channels [16]. SWCNTs were previously proposed as unique probes for imaging of the whole animal [17] and for intracellular single molecule tracking in cultured cells [18]. In our previous work, SWCNTs were injected intraventricularly in live rat pups and then individually followed as they diffused inside the ECS of acute slices. Tracking of SWCNTs provided simultaneous information on local dimensions and diffusion environment, revealing the ECS rheological properties and organisation at the nanoscale. In the same year, diffusion properties of the ECS in different brain areas were also explored by Zheng *et al.* [19] in young rat acute slices by combining time-resolved fluorescence anisotropy imaging with diffraction-limited two-photon excitation fluorescence microscopy. In particular, the team could extract the diffusivity (relative to free diffusion in artificial cerebrospinal fluid) inside the nanoscopic synaptic cleft of giant synapses, that could hence be resolved with the two-photon excitation microscope, formed by hippocampal mossy fibres on CA3 pyramidal cells [19]. Recently, images of the interstitial space detailing the live ultrastructure of the ECS were also obtained by Tønnesen *et al.* in organotypic brain slices [20]. The authors presented a quantitative analysis of the ECS structures and revealed structural dynamics in response to a variety of stimuli using an elegant approach termed STED-powered super-resolution shadow imaging (SUSHI). All these exciting methods have improved dramatically our possibilities to study the ECS and to unravel its interplay with processes at the molecular level.

Here we expand the method presented in Godin *et al.* for rat pups [13] by analysing single-nanotube trajectories in (*i*) organotypic brain slices, a highly versatile preparation that allows easy genetic and pharmacological manipulation, and (*ii*) acute brain slices from adult mice, a classic preparation in neuroscience physiology. This sets the foundation stone for the exploration of the ECS at super-resolution level in adult live brain tissue, relevant for studying physiology, aging and brain disorders.

2. Material and methods

2.1. SWCNT preparation

1 mg of HiPco synthesized nanotubes (batch no. 195.7, from Rice University) was suspended with 50 mg of monofunctional phospholipid-polyethylene glycol (PL-PEG) molecules (#mPEG-DSPE-5000, Laysan Bio) in 10 ml of deuterium oxide (Sigma Aldrich). The above solution was then sonicated for 30 min in water bath until full dissolution and then homogenised for 15 min at 19,000 rpm. SWCNTs were further dispersed by tip sonication (20 W for 8 min). Nanotube bundles and impurities were precipitated by centrifugation at 3,000 rpm for 60 min at room temperature. 70–80% of the supernatant was then collected and stored at 4 °C. PL-PEG functionalised SWCNTs can be stored at 4 °C for 1 month before tissue delivery. The concentration of the PL-PEG SWCNT stock solution was estimated to be ~ 10 mg/l. The subpopulation of SWCNTs with a (6,5) chirality which are imaged in this work, was estimated at 3–5% of the total SWCNT solution [13].

2.2. Animal models

2.2.1. Rat organotypic cultures and nanotube incubation

Organotypic slice cultures were prepared as previously described [21]. Hippocampal slices (350 µm) were obtained from postnatal day 5 to postnatal day 7 Sprague-Dawley rats using a McIlwain tissue chopper and were placed in a pre-heated (37 °C) dissection medium containing (in mM): 175 sucrose, 25 D-glucose, 50 NaCl, 0.5 $CaCl_2$, 2.5 KCl, 0.66 KH_2PO_4, 2 $MgCl_2$, 0.28 $MgSO_4$-$7H_2O$, 0.85 Na_2HPO_4-$12H_2O$, 2.7 $NaHCO_3$, 0.4 HEPES, 2 × 10–5% phenol red, pH 7.3 (all products from Sigma unless specified). After 25 min of incubation, slices were transferred on white hydrophilic polytetrafluoroethylene (FHLC) membranes (0.45 µm, Millipore) set on Millicell Cell Culture Inserts (Millipore, 0.4 mm; Ø 30 mm), and cultured for up to 14 days on multiwell-plates at 35 °C / 5% CO_2 in a culture medium composed of 50% Basal Medium Eagle, 25% Hank's balanced salt solution 1× (with $MgCl_2$ / with $CaCl_2$), 25% heat-inactivated horse serum, 0.45% D-glucose, 1 mM L-glutamine (all products from Gibco unless specified). The medium was changed every 2–3 days.

For SWCNT incubation, 3 µl of nanotubes solution was mixed with 10 µl of culture medium and incubated with the slices for 2 h at 35 °C / 5% CO_2 (Fig. 1a). Slices were imaged in HEPES-based artificial cerebrospinal fluid (aCSF) containing (in mM): 130 NaCl, 2.5 KCl, 2.2 $CaCl_2$, 1.5 $MgCl_2$, 10 HEPES, and 10 D-glucose, for up to 1 h at a controlled temperature (Fig. 1c). A total of 22 nanotubes were recorded over 9 slices from 5 dissected animals (n = 5).

2.2.2. Injection of nanotubes in adult mice and acute brain slice preparation

6 µl of SWCNT solution were injected into the cerebral lateral ventricle of 6-months-old C57BL/6J mice (Charles River) by stereotactic surgery (coordinates from bregma: −0.5 mm anteroposterior, 1 mm mediolateral, −2.4 dorsoventral). Inoculation was performed under deep isoflurane anaesthesia at a flow rate of 1 µl/min with a 30-gauge Hamilton syringe coupled to a microinjection pump (World Precision Instruments). The needle was left in place for 10 min to avoid leakage, and then slowly retracted. Animals received buprenorphine (0.1 mg/kg) as analgesic and returned to their cages. The Institutional Animal Care and Use Committee of Bordeaux (CE50) approved experiments under license number APAFIS#5520-2016052514328805.

1–2 h after injection of the nanotubes, mice were euthanized by cervical dislocation. Brains were extracted and coronal sections (300 µm thick) were prepared in a VT1200S vibratome (Leica) in ice-cold low-Na^+ low-Ca^{2+} high-Mg^{2+} aCSF solution containing (in mM) 180 sucrose, 2.5 KCl, 1.2 NaH_2PO_4, 10 glucose, 26 $NaHCO_3$, 20 HEPES, 10 $MgSO_4$ and 0.5 $CaCl_2$. Slices were then transferred to oxygenated aCSF (gassed with 95% O_2, 5% CO_2, pH = 7.4) with the following composition (in mM) 126 NaCl, 2.5 KCl, 1.2 NaH_2PO_4, 26 $NaHCO_3$, 10 glucose, 3 sodium pyruvate, 2 $MgSO_4$ and 2 $CaCl_2$ and kept at room temperature and 5% CO_2 until imaged (Fig. 1b). Images were collected at 37 °C in a 3D-printed chamber with controlled temperature and CO_2. Warmed aCSF was perfused throughout data collection by a peristaltic pump. Slices were imaged for no more than 1 h (Fig. 1c). A total of 6 nanotubes (recording times typically last 10–20 min per SWCNT) were analysed from 3 euthanized animals (n = 3).

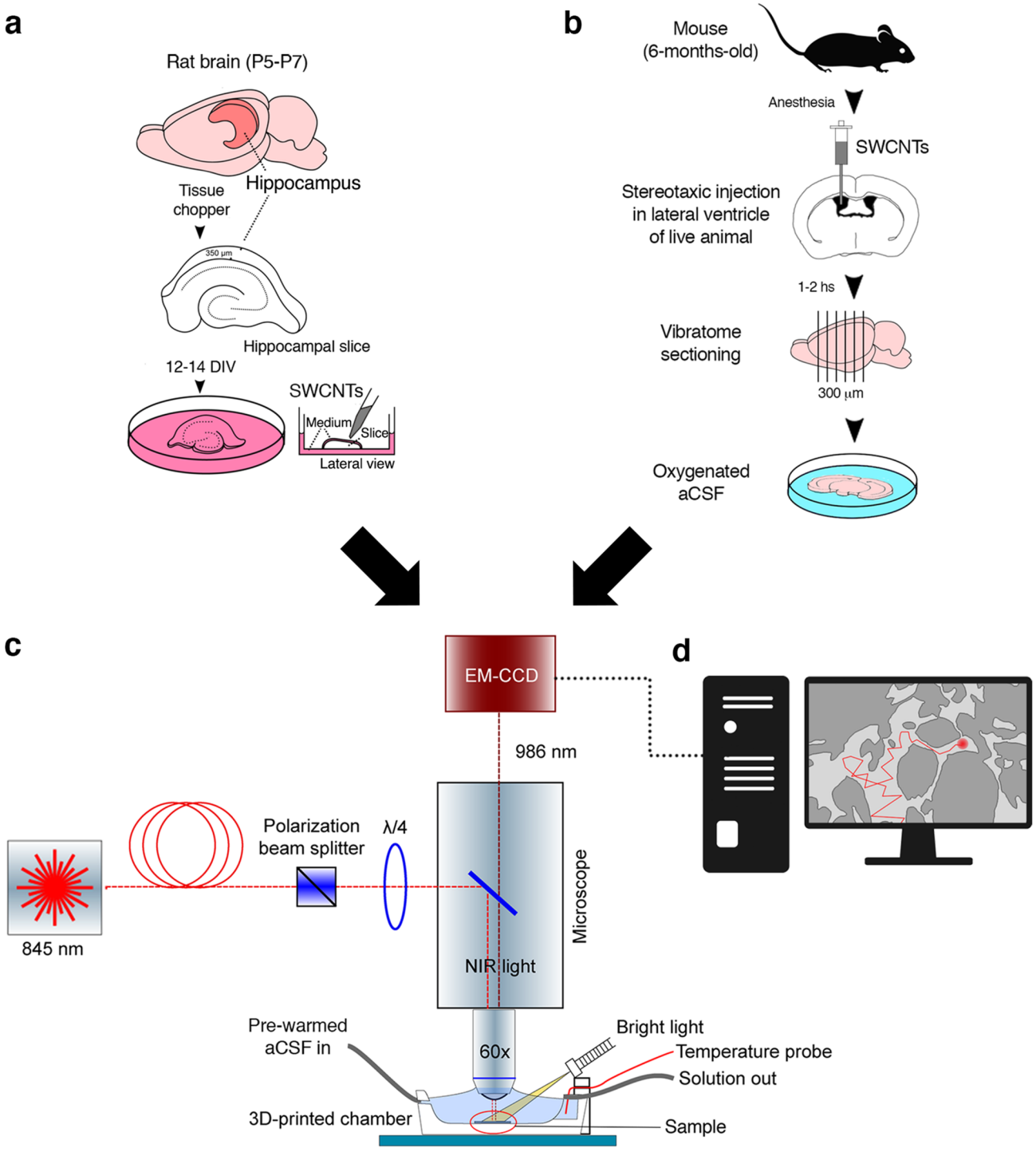

Fig. 1. Schematic of the experimental setup. a) Rat organotypic culture and SWCNT incubation: hippocampal organotypic slices were prepared from rat pup brains and cultured for 12–14 days *in vitro* (DIV) before SWCNT incubation; b) Acute brain slice preparation and SWCNT injection: adult mice were injected intraventricularly with SWCNTs; acute brain slices were prepared after 1–2 h; c) NIR imaging in the ECS of live tissues: Circularly polarized NIR light was applied to the slice through a 60× immersion objective. Emission light was collected through a long-pass filter to receive the 986 nm light from the (6,5) SWCNTs. Images were acquired with a water-cooled EM-CCD camera. Tissue was maintained at physiological extracellular milieu composition and temperature during acquisition time. Tissue integrity was constantly checked through oblique illumination with a white light.

2.3. Near infrared (NIR) imaging

Imaging of freely moving SWCNTs in ECS was performed on a customized upright epifluorescent microscope (Nikon) equipped with an EMCCD camera (ProEM-HS, Princeton Instrument). A 845 nm laser (Coherent) was used to excite the (6,5) SWCNTs at a phonon sideband. This excitation is optimal for signal-to-noise ratio and to ensure tissue integrity [22]. The free-space laser was fibre-coupled into a single mode end-polished fibre and then directed towards a polarisation beam splitter (Fig. 1c). A quarter-wave plate was used to obtain a circular-polarised excitation. Incident light was directed onto the samples with an 875 nm dichroic filter (Semrock), while emission light was filtered out with a long pass 900 nm filter (Semrock). To check the overall quality of the tissue, a standard white light fibre was positioned above

the sample at an angle of ~30°. A standard 4× objective (NA 0.1, Nikon) was initially used to check the position in the entire slice and determine the brain region to be imaged. Images were collected at a controlled temperature with a water immersion 60× objective (water immersion, NA 1.0, Nikon) using an exposure time of 30 ms (Fig. 2a).

2.4. Image analysis

Image analysis was performed using custom MATLAB (MathWorks) and Python scripts unless specified otherwise.

2.4.1. Single-molecule localization

Analysis of individual diffusing SWCNTs in the ECS of live tissues was performed as previously described with minor modifications [13]. Briefly, the localisation of the SWCNTs was initially determined by analysing the images with MetaMorph software (Molecular Devices). Super-localization of the SWCNT centroids was then obtained by fitting the images with two-dimensional asymmetric Gaussian functions having arbitrary orientations. MetaMorph Software was used to provide nanotube locations as initial fitting guess in MATLAB. Three consecutive images were averaged for each fit to improve the localization precision (~50 nm in water). SWCNT coordinates were then interconnected to reconstruct nanotube trajectories. When present over the recording, drifts due the peristaltic flux or to the movement of the slice being imaged were removed using slowly evolving non-Brownian component within the SWCNT trajectory, or when available, using immobile SWCNTs present in the field of view (Fig. 2a-b).

For each trajectory, the SWCNT length was estimated using the distribution of the longest axis of the 2D asymmetric Gaussian fits constructed when SWCNT movements were undetectable (nanotubes

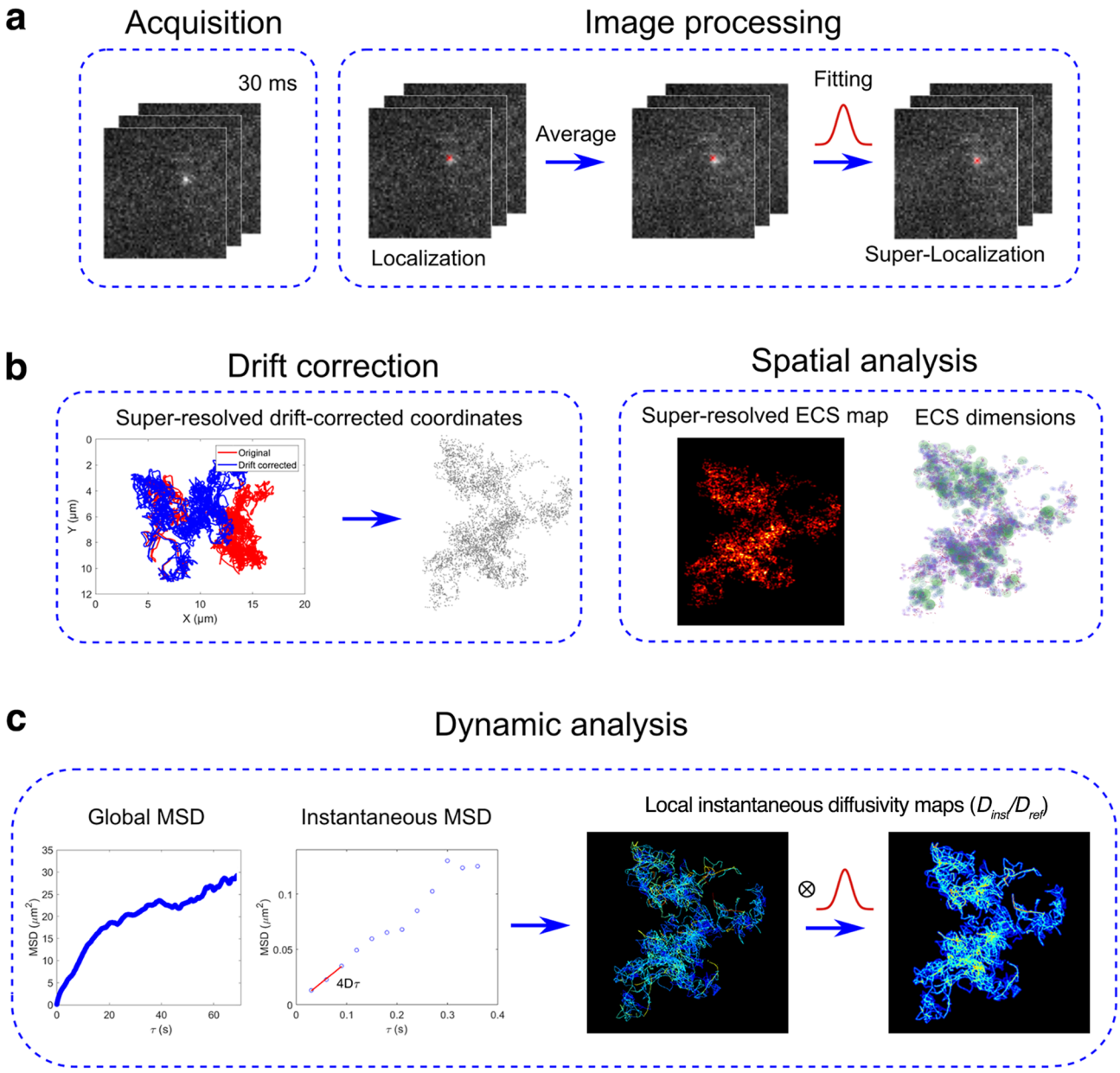

Fig. 2. Schematic of image analysis. a) 30 ms rate consecutive frames were acquired (~5000 localizations in total). In each image, the localization of the SWCNT was obtained, averaged and fitted to create a super-resolved image. b) Drift correction provided the precise super-resolved trajectory coordinates. This allowed the reconstruction of the super-resolved maps and calculation of ECS dimensions perpendicular to the nanotube path. c) Global MSDs and instantaneous diffusion constants were calculated using a sliding windows of 450 ms. Local relative diffusivity maps were created based on the trajectories in panel (b). Upper and lower values were adjusted to fix a standard colour scale, to allow comparison of different maps.

are considered immobile for displacements between images < 40 nm). More precisely, the length was obtained using the mean of the long axis distribution corrected by the point-spread function of the microscope and the exciton diffusion length of ~100 nm to take into account non-emitting nanotube ends [13,14,23].

2.4.2. Estimation of ECS dimensions and super-resolved images

For each trajectory, a super-resolved image of the ECS was computed by cumulating the SWCNT localizations (typically 5000 points) and convoluting them with a two-dimensional Gaussian of 50 nm width and unit amplitude (Fig. 2b). For visualization purposes, these images were created using pixels of 25 nm. Area covered by SWCNTs exploration was calculated by measuring the area of binary images obtained by thresholding (Min Error) the super-resolved maps in ImageJ (NIH).

The local dimensions of the ECS were then estimated by analysing the "shape" of the local area explored by SWCNTs along their trajectory. More specifically, in a given time window, the area describing nanotube localizations was fitted to an ellipse. The shorter dimension of this ellipse was then used to define local ECS dimensions, denoted by ξ, when the ellipse shape (i.e. its short axis) was constrained by the diameter of the local "channel" in which the SWCNT is diffusing. In order to rationally identify such confinement and thus select the time window duration (i.e. the number of data points in the time window) at which ξ can be determined, we proceeded as follows: we simulated trajectories mimicking SWCNT free diffusion, and, as above, we fitted simulated nanotube localization over a range of time window durations with ellipses to compute the ellipse eccentricity (where an eccentricity of zero corresponds to a circularly shaped distribution, and an eccentricity of one to a distribution along a straight line). We then calculated the ratio between the experimental ellipse eccentricity to the simulated eccentricities, as a function of the time window duration (Fig. S1): an eccentricity ratio greater than one indicates that experimental nanotube lateral diffusion is restricted by its environment. As expected for most datasets, when increasing the time window duration, the eccentricity ratio starts at a value greater than 1 and increases for window sizes up to 6 data points. It then decreases back towards unity, which it reaches for window sizes from ~30 data points. This behaviour can be easily interpreted as follows: at short time scales (up to 6 data points), SWCNT diffusion is highly constrained laterally by a confining ECS channel; thus, a diffusing SWCNT locally explores an area having a more elongated shape than a freely diffusing particle. At longer time scales (from ~30 data points), however, the nanotube disengages from local confining channels and the overall explored area takes a shape similar to freely diffusing particles. This analysis thus indicated that the effect of the local confining channels starts to dissipate after a time interval of ~6 points, i.e. 180 ms. We thus chose to use local windows of 6 data points to estimate the width of the local environment (defined along the small axis of ellipses), and report these widths as ξ, the local dimensions of the ECS along the nanotube trajectories (Fig. 2b).

2.4.3. Local relative diffusivity and ECS effective viscosity

For each trajectory, the mean square displacement (MSD) was calculated as a function of time intervals Δt, set as multiples of the frame integration time following the methods of Kusumi *et al.* [24]. For short time delays , the two-dimensional *MSD* can be approximated by a linear slope:

$$MSD(\Delta t) = 4D_{inst}\,\Delta t$$

allowing to define D_{inst}, the instantaneous diffusion coefficient. Therefore, D_{inst} can be directly estimated by linearly fitting the *MSD*-Δt plot over short period of times, (90 ms) (Fig. 2c).

Spatial diffusion maps could be calculated from the *local* instantaneous MSD values along each trajectory (Fig. S2), over a sliding window of 450 ms. Linear fits of the MSD slopes were then applied to the first 90 ms to obtain the instantaneous diffusion coefficients as a function of time (Fig. 2c). Values falling within the same pixels were averaged (Fig. S2).

In our prior work [13], a "local effective ECS viscosity", η_{inst},was defined and deduced from local values of D_{inst}, the nanotube length and diameter [25]. Because η_{inst} was calculated on finite sliding windows (and not on infinitely short times due to imaging speed limited to video rates), SWCNT motions were likely to be not purely Brownian in the time windows. This implies that local ECS geometrical tortuosity and hydrodynamic drag experienced by the diffusing object near cellular interfaces in narrow ECS channels contribute to increase experimental η_{inst} values which are thus distinct from the intrinsic viscosity of the ECS fluid [26]. Extracting the local intrinsic viscosity of the ECS fluid (which contains contributions from ECS macromolecules) from SWCNT trajectories is thus a complex task that will require future development beyond this work. Instead, here we defined a *local* relative diffusivity (D_{inst}/D_{ref}) using a similar approach as proposed on *macroscopic* studies [1,5,19,26], where D_{ref} is the free diffusion of the considered SWCNT in a fluid having the viscosity of the cerebrospinal fluid (CSF):

$$D_{ref} = \frac{[3k_B T ln(2\varphi)]}{8\pi\eta_{ref} L}$$

where φ is the SWCNT aspect ratio, and L is the nanotube length. A related parameter defined as tortuosity (to account for the increase of path length, dead-ends, local interactions) was sometime defined as the reciprocal of the square of the relative diffusivity [1]. For visualization purposes of the spatial diffusivity maps, convolution with a 2D Gaussian of 50 nm full width at half maxima (FWHM) was applied to smooth the data (Fig. 2c).

3. Results and discussion

3.1. Single-molecule tracking of SWCNTs in the ECS of live brain tissue

SWCNTs were used to probe the ECS of different brain tissue models at the nanoscale level. SWCNTs were initially functionalised with PL-PEG molecules, to prevent non-specific biomolecule adsorption and minimise their sticking onto biologicals structures [27]. PL-PEG coated SWCNTs also displayed very low cytotoxicity while still being highly luminescent, an essential condition for bio-imaging and tracking over long period of time [27]. The spectral range of PL-PEG-coated SWCNTs with a (6,5) chirality (845 nm to excite the phonon sideband and emission at 986 nm) falls within the transparency window of neural tissue (NIR region, [12]). Different cameras (e.g. the InGaAs technology) could be also used to detect other nanotube chiralities using the same excitation wavelength. This method could potentially reveal a higher number of SWCNTs.

SWCNTs were delivered into brain tissues, either by incubation (organotypic slices) or injection into the cerebral lateral ventricle of live adult mouse (acute slices). Both methods guaranteed minimal tissue damage and inflammation [13]. Individual SWCNTs were detected in diverse areas of the brain slice: CA1 and dentate gyrus (DG) in rat hippocampal organotypic slices; cortex, striatum, hippocampus and ventral midbrain in mouse acute slices. Interestingly, finding suitable nanotubes for tracking in adult mouse acute slices was more challenging than in rat organotypic slices. This might be due not only to the increased tissue complexity of acute slices, but also to the significantly larger distances that a SWCNT travels in a whole brain (adult mouse) rather than in a hippocampal slice (rat organotypic). Moreover, organotypic slices can be incubated with large volumes of SWCNT solution, while in the live mouse the amount of liquid to inject is limited. This means that in cultured slices, the volume density of SWCNTs observed in the tissue is significantly higher than in acute slices. Incubating acute slices with the SWCNT solution might solve the problem, but medium oxygenation (imperative to keep intact the fine structures of the ECS) strongly complicates SWCNT penetration.

Imaging was performed at different depths in the slice, ranging from 10 µm up to ~70 µm (Fig. S3a). A white light lamp under oblique illumination was used to obtain a visible image of the slice and to discern the cell bodies in the field of view. Although the quality of the tissue was checked before each SWCNT recording, the first 10 µm of tissue were always discarded to exclude the first cell layer potentially damaged by the preparation. Indeed, investigation of the fine architecture of the ECS requires the best preservation of the cellular structures. Slices were imaged up to 1 h and then discarded, allowing tracking typically two SWCNTs per slice, during several minutes per nanotube. SWCNTs could be imaged deeper in the tissue in organotypic compared to acute slices, although this difference was not significant (Fig. S3a). This might be due to the increased cell density and tissue complexity characteristic of acute slices. The detection of other SWCNT chiralities emitting in the 1–1.5 µm range where tissues are more transparent using InGaAs cameras should allow deeper imaging.

The luminescence of the nanotubes was recorded for several minutes (up to 20 min) with excellent photostability and no visible photodamage to the tissue. Indeed, the combination of their length and rigidity can moderate their diffusion rates to be compatible with video-rate recording (Movie S1). For each recorded frame, the 2D Gaussian fitting analysis allowed the extraction of the nanotube centroid and orientation with subwavelength precision (~50 nm). SWCNTs going out of focus while being tracked were analysed as separate trajectories. Analysis of the 2D Gaussian asymmetry gave measurements of nanotube lengths. A total of 28 nanotubes where analysed in this study, rendering 278,029 organotypic and 70,175 acute mouse SWCNT segments of "instantaneous" localizations. The length distribution of the nanotubes was centred around 500 nm with very few outliers, confirming the consistency and reproducibility of the nanotube preparation (Fig. S3b).

3.2. Brain ECS dimensions in different animal models

The diffusion of a nanotube throughout the ECS is inherently constrained, among other factors, by the geometry of the explored compartment [1]. Thus, by tracking an individual SWCNT trajectory, it is possible to estimate the dimensions of this compartment, providing structural information of the ECS with nanometre precision.

We computed super-resolved images of the ECS for both rat organotypic and mouse acute slices. Super-resolved maps revealed a highly heterogeneous and tortuous ECS in both tissue models (Fig. 3a). The area covered by the SWCNT exploration was vastly heterogeneous, ranging from 2 to 80 µm^2 (Fig. 3b). SWCNTs tended to explore more extended areas in organotypic slices (mean = 30.5 ± 5.5 µm^2 organotypic vs. 17.7 ± 6.6 µm^2 adult mouse acute).

Transverse ECS dimensions ξ were determined from the analysis of the local areas explored by single diffusing SWCNTs. The resulting maps of ξ (Fig. 3c) revealed a wide range of dimensions, stretching from 50 to 400 nm (Fig. 3d). Despite this heterogeneity, 50% of ECS widths were between 80 and 220 nm. These numbers are in accordance with previous data obtained from electron microscopy of cryo-fixed tissue [2] and STED microscopy (SUSHI) in live tissue [20].

Distribution analysis of ξ revealed potentially different ECS local dimensions between mouse acute slices and organotypic tissues, the latter displaying a longer tail of large local dimensions. This might be

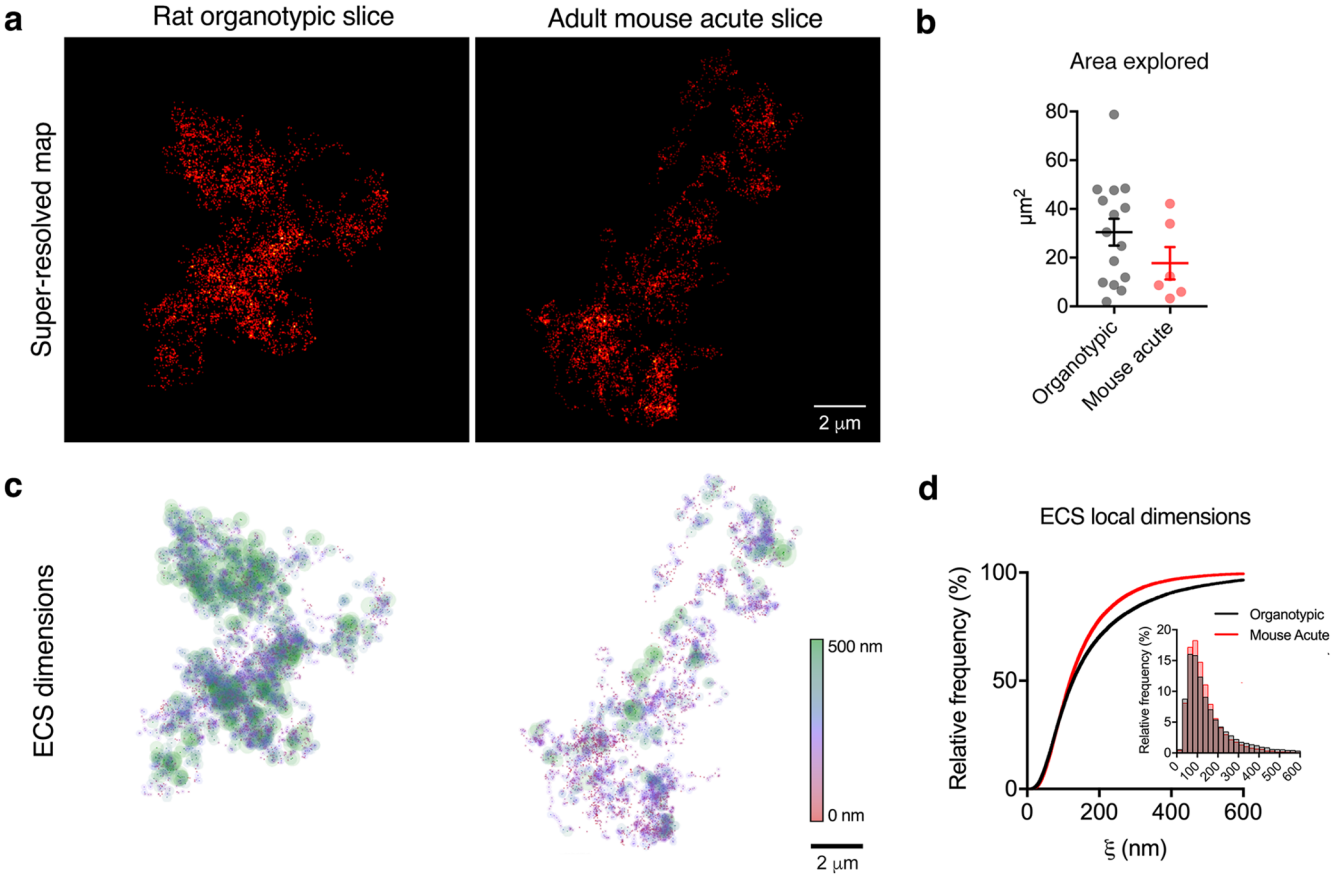

Fig. 3. Spatial analysis. a) Examples of super-resolved images obtained from individual SWCNTs freely diffusing in the ECS of a rat organotypic slice and an adult mouse acute slice (~5000 localizations, respectively). Scale bar = 2 µm. b) Area explored from the totality of SWCNTs tracked in the two models. Data is expressed as mean ± SEM. c) Maps of local dimensions from the super-resolved SWCNT localizations presented in (a). Maps were drawn by plotting at each localization a circle of size and colour corresponding to the local dimension ξ. Scale bar = 2 µm. d) Cumulative frequency distributions of ECS transverse dimensions ξ from the totality of SWCNTs tracked in this study. Inset: Frequency distribution of the ECS widths, using a bin size of 50 nm.

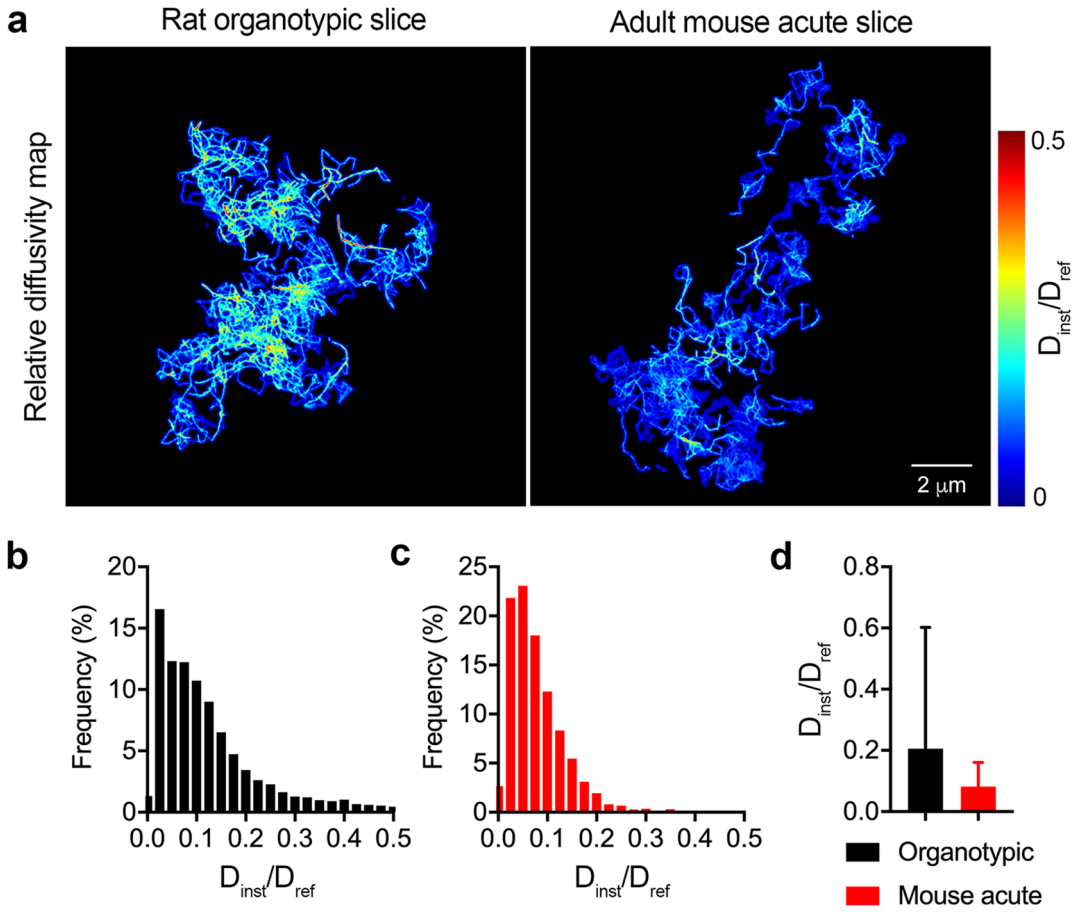

Fig. 4. Analysis of ECS dynamics. a) Spatial maps of the instantaneous relative diffusivity coefficients obtained from individual SWCNTs freely diffusing in the ECS of a rat organotypic slice and an adult mouse acute slice. b and c) Frequency distributions of instantaneous relative diffusivity coefficients calculated over the totality of SWCNTs used in this study (black: organotypic slices; red: mouse acute slices. d) Summary of relative diffusivities calculated over the totality of SWCNTs used in this study (mean ± SD). (For interpretation of the references to colour in this figure legend, the reader is referred to the web version of this article.)

due to the immaturity of the extracellular matrix in the younger brain (organotypic slices) [28,29], probably resulting in looser cell attachments and hence larger dimensions. In both datasets, the 25th percentile of local dimensions is ~80 nm, whereas the median is 120 nm for mouse acute slices and 130 nm for rat organotypic tissues, and the 75th percentile is 190 nm for mouse acute slices and 220 nm for rat organotypic tissues. (Fig. 3d). The larger ξ found in organotypic slices is in accordance with previous studies reporting increased ECS volume fractions in the young brain compared to adult [30,31]. It should be noted, however, that ECS widths ξ might not always correlate with the ECS volume fraction, ξ being a local parameter and not a global magnitude like the ECS volume. More studies directly comparing young and adult mouse tissue with super-resolution imaging are needed to draw an unambiguous conclusion.

3.3. SWCNTs diffusion properties in the brain ECS of different animal models

One of the main advantages of SWCNT tracking is that diffusion information can be obtained simultaneously with ECS dimensions. Maps of the instantaneous diffusion constants (D_{inst}, Fig. S2) and therefore local diffusivities (D_{inst}/D_{ref}, Fig. 4a) were calculated using a 450 ms sliding window along the global MSDs. Immobile SWCNTs were identified from their characteristic plateau-shape behaviour of the global MSD and discarded from the analysis (Fig. S4).

Local instantaneous diffusivity maps revealed that both models displayed spatially heterogeneous diffusion patterns (Fig. 4a), confirming the rheological diversity of the brain ECS. In rat organotypic hippocampal slices, local diffusivity had a mean of 0.21 (median = 0.11) with broad standard deviation (0.39, Fig. 4b) whereas in adult mouse acute slices, D_{inst}/D_{ref} had a mean of 0.08 (median = 0.06, standard deviation = 0.07, Fig. 4c). Overall, higher local diffusivity values were found in organotypic than in acute slices (Fig. 4d). These results are consistent with observations that even if organotypic hippocampal slices maintain some of the characteristic features of the brain circuits, they do not achieve the complexity of an *in vivo* model [32]. In principle, the local diffusivity values measured here can be compared to other rheological measurements such as performed by Zheng *et al.* [19] in live brain tissue, yet with more macroscopic resolution. This comparison yields smaller diffusivities than in [19]. As mentioned above, diffusivity does not only reflect the ECS fluid viscosity but it also contains contributions of the ECS tortuosity [26]. The latter includes geometric tortuosity, and wall drag in narrow ECS channels (sometimes referred as viscous tortuosity) which is a function of the hydrodynamic dimension of diffusing objects. This implies that diffusivity is defined for each type of object and absolute values between different types of nanoprobes are difficult to compare (with lower diffusivities for larger objects). The recent development of fluorescent ultrashort SWCNTs [22] might provide future opportunities to bridge the gap between small “0D” molecular probes and the 1D SWCNTs.

Importantly, having access to the local (i.e. spatially resolved) SWCNT diffusivity provides novel insights about the heterogeneity of the diffusion environment of the ECS that macroscopic methods cannot reveal. In particular, although space constriction may play a role in the local viscosity by concentrating different ECS components, we found

that local diffusivity values do not necessarily correlate with ECS dimensions [13]. For instance, low diffusivity areas can be observed in rat organotypic slices and high diffusivity areas can be observed in mouse adult acute slices while it is known that the density of the extracellular matrix is more complex in adult compared to young brain [28,29] which might imply lower diffusivity due to higher spatial constriction. This observation thus suggests that an active regulation of the ECS diffusion properties takes place in the different brain tissue models. Interestingly, it has also been recently observed that in several neurological diseases (e.g. schizophrenia) not only the ECS dimensions are altered [1] but also the ECS matrix components [33]. An example of this phenomenon is illustrated by the perineuronal nets, a component of the extracellular matrix surrounding certain populations of neurons, which are lost in schizophrenia mouse models to varying degrees depending on the brain region observed [34].

4. Conclusion and perspectives

Deep-tissue super-localization microscopy based on tracking individual moving objects represents a unique approach in neuroscience. Here, we reinforce the concept that SWCNTs are the ideal nano-probes to unveil the morphology and diffusive environment of the ECS in brain tissue. SWCNTs were used to explore the brain ECS in different animal models, giving remarkable details at the nanoscale level. Indeed, their nanometre scale diameter gave unusual accessibility in the complex ECS environment of both young rat and adult mouse brains. The ECS was found to be a maze of heterogeneous compartments bearing specific rheological properties, ranging from low to high local diffusivity. Our observations particularly suggest that ECS rheology may depend on brain regions and developmental state. We believe SWCNTs will undoubtedly be useful to thoroughly explore these hypotheses. Given the compiling evidences demonstrating the differences between rat and mouse models [35], it may be of interest to explore the possibility of distinct ECS rheology between species. In addition to unveiling the ECS features at a super-resolution level, single-nanotube tracking together with other labelling strategies will enable targeting specific unexplored compartments, such as the synaptic cleft or the perineuronal milieu. Furthermore, information on the ECS network at the nanoscale will foster further strategies for genetic manipulation and pharmacological delivery. The acquired knowledge will also influence the understanding on chemical-based neural communication and synaptic connectivity in both physiological and pathological conditions. The possibility to probe adult brain tissue paves the way to explore the ECS in aging and age-related disorders.

Acknowledgements

The University of Bordeaux and the Centre National de la Recherche Scientifique provided infrastructural support. This work was specifically supported by grants from the Agence Nationale de la Recherche (ANR-14-OHRI-0001-01, ANR-15-CE16-0004-03), IdEx Bordeaux (ANR-10-IDEX-03-02), the France-BioImaging National Infrastructure (ANR-10-INBS-04-01), and the Labex Brain Program (ANR-10-LABX-43). C.P. acknowledges funding from the European Union's Horizon 2020 research and innovation program under the Marie Skłodowska-Curie grant agreement No 793296. F.N.S. received a fellowship from the Basque Government postdoctoral program (Grant number POS_2017_2_005). J.S.F. would like to thank the IINS Cell Culture Facility, particularly Emeline Verdier for the help with the organotypic slices preparation. Animal experiments were performed at the Animal Facilities of the University of Bordeaux, supported by the Région Nouvelle-Aquitaine.

Appendix A. Supplementary data

Supplementary data to this article can be found online at https://doi.org/10.1016/j.ymeth.2019.03.005.

References

[1] E. Sykova, C. Nicholson, Diffusion in brain extracellular space, Physiol. Rev. 88 (4) (2008) 1277–1340.
[2] N. Korogod, C.C. Petersen, G.W. Knott, Ultrastructural analysis of adult mouse neocortex comparing aldehyde perfusion with cryo fixation, Elife 4 (2015).
[3] L. Xie, H. Kang, Q. Xu, M.J. Chen, Y. Liao, M. Thiyagarajan, J. O'Donnell, D.J. Christensen, C. Nicholson, J.J. Iliff, T. Takano, R. Deane, M. Nedergaard, Sleep drives metabolite clearance from the adult brain, Science 342 (6156) (2013) 373–377.
[4] F. Ding, J. O'Donnell, Q. Xu, N. Kang, N. Goldman, M. Nedergaard, Changes in the composition of brain interstitial ions control the sleep-wake cycle, Science 352 (6285) (2016) 550–555.
[5] C. Nicholson, S. Hrabetova, Brain extracellular space: the final frontier of neuroscience, Biophys. J. 113 (10) (2017) 2133–2142.
[6] Z. Liu, L.D. Lavis, E. Betzig, Imaging live-cell dynamics and structure at the single-molecule level, Mol. Cell 58 (4) (2015) 644–659.
[7] J.P. Heller, D.A. Rusakov, The nanoworld of the tripartite synapse: insights from super-resolution microscopy, Front. Cell. Neurosci. 11 (2017) 374.
[8] B. Cragg, Preservation of extracellular space during fixation of the brain for electron microscopy, Tissue Cell 12 (1) (1980) 63–72.
[9] M. Pallotto, P.V. Watkins, B. Fubara, J.H. Singer, K.L. Briggman, Extracellular space preservation aids the connectomic analysis of neural circuits, Elife 4 (2015).
[10] N. Ohno, N. Terada, S. Saitoh, S. Ohno, Extracellular space in mouse cerebellar cortex revealed by in vivo cryotechnique, J. Comp. Neurol. 505 (3) (2007) 292–301.
[11] D.A. Rusakov, L.P. Savtchenko, K. Zheng, J.M. Henley, Shaping the synaptic signal: molecular mobility inside and outside the cleft, Trends Neurosci. 34 (7) (2011) 359–369.
[12] C. Nicholson, L. Tao, Hindered diffusion of high molecular weight compounds in brain extracellular microenvironment measured with integrative optical imaging, Biophys. J. 65 (6) (1993) 2277–2290.
[13] A.G. Godin, J.A. Varela, Z. Gao, N. Danné, J.P. Dupuis, B. Lounis, L. Groc, L. Cognet, Single-nanotube tracking reveals the nanoscale organization of the extracellular space in the live brain, Nat. Nanotechnol. 12 (3) (2017) 238–243.
[14] L. Cognet, D.A. Tsyboulski, J.D. Rocha, C.D. Doyle, J.M. Tour, R.B. Weisman, Stepwise quenching of exciton fluorescence in carbon nanotubes by single-molecule reactions, Science 316 (5830) (2007) 1465–1468.
[15] S. Cambre, S.M. Santos, W. Wenseleers, A.R. Nugraha, R. Saito, L. Cognet, B. Lounis, Luminescence properties of individual empty and water-filled single-walled carbon nanotubes, ACS Nano 6 (3) (2012) 2649–2655.
[16] N. Fakhri, F.C. MacKintosh, B. Lounis, L. Cognet, M. Pasquali, Brownian motion of stiff filaments in a crowded environment, Science 330 (6012) (2010) 1804–1807.
[17] K. Welsher, Z. Liu, S.P. Sherlock, J.T. Robinson, Z. Chen, D. Daranciang, H. Dai, A route to brightly fluorescent carbon nanotubes for near-infrared imaging in mice, Nat. Nanotechnol. 4 (11) (2009) 773–780.
[18] N. Fakhri, A.D. Wessel, C. Willms, M. Pasquali, D.R. Klopfenstein, F.C. MacKintosh, C.F. Schmidt, High-resolution mapping of intracellular fluctuations using carbon nanotubes, Science 344 (6187) (2014) 1031–1035.
[19] K. Zheng, T.P. Jensen, L.P. Savtchenko, J.A. Levitt, K. Suhling, D.A. Rusakov, Nanoscale diffusion in the synaptic cleft and beyond measured with time-resolved fluorescence anisotropy imaging, Sci. Rep. 7 (2017) 42022.
[20] J. Tonnesen, V. Inavalli, U.V. Nagerl, Super-resolution imaging of the extracellular space in living brain tissue, Cell 172 (5) (2018) 1108.e15–1121.e15.
[21] L. Stoppini, P.A. Buchs, D. Muller, A simple method for organotypic cultures of nervous tissue, J. Neurosci. Methods 37 (2) (1991) 173–182.
[22] N. Danné, M. Kim, A.G. Godin, H. Kwon, Z. Gao, X. Wu, N.F. Hartmann, S.K. Doorn, B. Lounis, Y. Wang, L. Cognet, Ultrashort carbon nanotubes that fluoresce brightly in the near-infrared, ACS Nano (2018).
[23] L. Oudjedi, A.N. Parra-Vasquez, A.G. Godin, L. Cognet, B. Lounis, Metrological investigation of the (6,5) carbon nanotube absorption cross section, J. Phys. Chem. Lett. 4 (9) (2013) 1460–1464.
[24] A. Kusumi, Y. Sako, M. Yamamoto, Confined lateral diffusion of membrane receptors as studied by single particle tracking (nanovid microscopy). Effects of calcium-induced differentiation in cultured epithelial cells, Biophys. J. 65 (5) (1993) 2021–2040.
[25] Y. Han, A. Alsayed, M. Nobili, A.G. Yodh, Quasi-two-dimensional diffusion of single ellipsoids: aspect ratio and confinement effects, Phys. Rev. E: Stat. Nonlinear Soft Matter Phys. 80 (1 Pt 1) (2009) 011403.
[26] D.A. Rusakov, D.M. Kullmann, Geometric and viscous components of the tortuosity of the extracellular space in the brain, Proc. Natl. Acad. Sci. U.S.A. 95 (15) (1998) 8975–8980.
[27] Z. Gao, N. Danné, A.G. Godin, B. Lounis, L. Cognet, Evaluation of different single-

walled carbon nanotube surface coatings for single-particle tracking applications in biological environments, Nanomaterials (Basel) 7 (11) (2017).
[28] C.E. Bandtlow, D.R. Zimmermann, Proteoglycans in the developing brain: new conceptual insights for old proteins, Physiol. Rev. 80 (4) (2000) 1267–1290.
[29] W. Su, S. Matsumoto, B. Sorg, L.S. Sherman, Distinct roles for hyaluronan in neural stem cell niches and perineuronal nets, Matrix Biol. (2018).
[30] H.F. Cserr, M. DePasquale, C. Nicholson, C.S. Patlak, K.D. Pettigrew, M.E. Rice, Extracellular volume decreases while cell volume is maintained by ion uptake in rat brain during acute hypernatremia, J. Physiol. 442 (1991) 277–295.
[31] A. Lehmenkuhler, E. Sykova, J. Svoboda, K. Zilles, C. Nicholson, Extracellular space parameters in the rat neocortex and subcortical white matter during postnatal development determined by diffusion analysis, Neuroscience 55 (2) (1993) 339–351.
[32] C. Humpel, Organotypic brain slice cultures: a review, Neuroscience 305 (2015) 86–98.
[33] G. Matuszko, S. Curreli, R. Kaushik, A. Becker, A. Dityatev, Extracellular matrix alterations in the ketamine model of schizophrenia, Neuroscience 350 (2017) 13–22.
[34] H.M. van 't Spijker, J.C.F. Kwok, A sweet talk: the molecular systems of perineuronal nets in controlling neuronal communication, Front. Integr. Neurosci. 11 (2017) 33.
[35] B. Ellenbroek, J. Youn, Rodent models in neuroscience research: is it a rat race? Dis. Model Mech. 9 (10) (2016) 1079–1087.